Helmholtz-Zentrum Dresden-Rossendorf (HZDR)

HZDR
HELMHOLTZ ZENTRUM
DRESDEN ROSSENDORF

# Efficient ion-slicing of InP thin film for Si-based hetero-integration

Lin, J.; You, T.; Wang, M.; Huang, K.; Zhang, S.; Jia, Q.; Zhou, M.; Yu, W.; Zhou, S.;
Wang, X.; Ou, X.;

Originally published:

October 2018

**Nanotechnology 29(2018)50, 504002**

DOI: https://doi.org/10.1088/1361-6528/aae281

Perma-Link to Publication Repository of HZDR:

https://www.hzdr.de/publications/Publ-28439

Release of the secondary publication
on the basis of the German Copyright Law § 38 Section 4.

Nanotechnology

**ACCEPTED MANUSCRIPT**

# Efficient ion-slicing of InP thin film for Si-based hetero-integration

To cite this article before publication: Jiajie Lin *et al* 2018 *Nanotechnology* in press https://doi.org/10.1088/1361-6528/aae281

Manuscript version: Accepted Manuscript

Accepted Manuscript is "the version of the article accepted for publication including all changes made as a result of the peer review process, and which may also include the addition to the article by IOP Publishing of a header, an article ID, a cover sheet and/or an 'Accepted Manuscript' watermark, but excluding any other editing, typesetting or other changes made by IOP Publishing and/or its licensors"

This Accepted Manuscript is **© 2018 IOP Publishing Ltd**.

During the embargo period (the 12 month period from the publication of the Version of Record of this article), the Accepted Manuscript is fully protected by copyright and cannot be reused or reposted elsewhere.
As the Version of Record of this article is going to be / has been published on a subscription basis, this Accepted Manuscript is available for reuse under a CC BY-NC-ND 3.0 licence after the 12 month embargo period.

After the embargo period, everyone is permitted to use copy and redistribute this article for non-commercial purposes only, provided that they adhere to all the terms of the licence https://creativecommons.org/licences/by-nc-nd/3.0

Although reasonable endeavours have been taken to obtain all necessary permissions from third parties to include their copyrighted content within this article, their full citation and copyright line may not be present in this Accepted Manuscript version. Before using any content from this article, please refer to the Version of Record on IOPscience once published for full citation and copyright details, as permissions will likely be required. All third party content is fully copyright protected, unless specifically stated otherwise in the figure caption in the Version of Record.

View the article online for updates and enhancements.

This content was downloaded from IP address 129.100.58.76 on 24/09/2018 at 07:35

1 2 3 4 5 6 7 8 9 10 11 12 13 14 15 16 17 18 19 20 21 22 23 24 25 26 27 28 29 30 31 32 33 34 35 36 37 38 39 40 41 42 43 44 45 46 47 48 49 50 51 52 53 54 55 56 57 58 59 60

# Efficient ion-slicing of InP thin film for Si-based hetero-integration

Jiajie Lin,[1, 2#] Tiangui You,[1#] Mao Wang,[3] Kai Huang,[1] Shibin Zhang,[1, 2] Qi Jia,[1] Min Zhou,[1] Wenjie Yu,[1] Shengqiang Zhou,[3] Xi Wang[1] and Xin Ou[1*]

[1] State Key Laboratory of Functional Materials for Informatics, Shanghai Institute of Microsystem and Information Technology, Chinese Academy of Sciences, Shanghai 200050 P.R. China

[2] University of Chinese Academy of Sciences, Beijing 100049 P.R. China

[3] Institute of Ion Beam Physics and Materials Research, Helmholtz-Zentrum Dresden-Rossendorf, Dresden 01328 Germany

[#] These authors contribute equally to this work.

[*]Email: ouxin@mail.sim.ac.cn

Abstract

Integration of high quality single crystalline InP thin film on Si substrate has potential impact on Si-based photonics and high-speed electronics. In this work, the exfoliation of 634 nm crystalline InP layer from the bulk substrate was achieved by sequential implantation of He ions and H ions at room temperature. It is found that the sequence of He and H ions implantations has a decisive influence on the InP surface blistering and exfoliation, which only occurs in the InP pre-implanted with He ions. The exfoliation efficiency first increases and then decreases as a function of H ions fluence. With a kinetics analysis of the thermally activated blistering process, it suggests that the He and H ions sequential implantation can reduce the InP thin film splitting thermal budget dramatically. Finally, a high-quality 2-inch InP-on-Si (100) hetero-integration wafer was fabricated by He and H ions sequential implantation at room temperature in combination with direct wafer bonding.

Keywords: InP-on-Si, hetero-integration, ion-slicing, wafer bonding

## 1. Introduction

Monolithic integration of InP with Si substrate has attracted great interest thanks to the potential applications of combining InP based optoelectronic and high-speed electronic devices with the mature Si-based microelectronic circuits [1-3]. However, it is difficult to hetero-epitaxially grow high quality single crystalline InP thin film on Si substrate [4,5]. High density defects, e.g., the threading and misfitting dislocations, exist in the hetero-epitaxially grown InP thin film due to the lattice mismatch (8%) and thermal expansion coefficient mismatch (73.1%) between



Accepted Manuscript

1
2
3
4
5
6
7
8
9
10
11
12
13
14
15
16
17
18
19
20
21
22
23
24
25
26
27
28
29
30
31
32
33
34
35
36
37
38
39
40
41
42
43
44
45
46
47
48
49
50
51
52
53
54
55
56
57
58
59
60

InP and Si [1,6], which limit the performance and reliability of optoelectronic and high-speed electronic devices fabricated on the epitaxial layers.

Alternatively, the ion-slicing technology appears to enable the generic development of high-quality III-V semiconductors-on-Si hetero-integration by transferring the III-V layer from crystal wafers to Si substrates. Ion slicing technology was first proposed by Bruel in 1995, which has been successfully applied to the mass production of silicon-on-insulator (SOI) wafers [7]. For the exploration of ion-slicing technology, it is the priority to realize the surface blistering or exfoliation on the target crystal wafers by light elemental ion implantation (e.g., H, He ions implantation) combining with a post annealing process. In recent years, several efforts have been made to achieve InP-on-Si hetero-integration materials by ion-slicing and layer transferring process. The surface blistering or exfoliation of InP crystal wafers by either H or He ion implantation has been reported [8-10]. Unlike Si, the exfoliation behavior of InP is strongly depended on the ion implantation temperature. With single H ions implantation, the InP surface blistering or exfoliation only occurs in two special implantation temperature windows, i.e., a high implantation temperature window of 150°C-250°C and a low implantation temperature window of -20°C-20°C [9,11]. However, it is difficult to control the implantation temperature since it is sensitive to both of the physical contact between the target wafers and sample holders and the ion implantation flux [10]. In the case of He ions implantation, a InP layer was successfully transferred to Si substrate by He ions implantation at -15°C or 20°C with a fluence of $5\times10^{16}$ cm$^{-2}$. However, nearly half thickness of the transferred InP layer was heavily damaged due to the heavier He ion implantation with a high fluence and at low temperature. Furthermore, with single H or He ions implantation, a post-annealing at relatively high temperature of 200-400°C for long duration was required for the InP surface blistering or exfoliation [9-12]. This will further increase the thermal stress between InP layer and Si substrate due to the large thermal mismatch. Therefore, it is urgent to develop an efficient ion-slicing process at room temperature for the high quality wafers-scale InP-on-Si hetero-integration.

In this study, the efficient exfoliation of InP thin film has been demonstrated by co-implantation of He and H ions sequentially at room temperature. The sequential implantation reduces the total ion fluence and thermal budget for the InP-on-Si hetero-integration by ion-slicing and layer transferring process. Combining with the direct wafer bonding, a high quality 2-inch InP-on-Si hetero-integration wafer was successfully fabricated.

## 2. Experimental details

He ions implantation with an energy of 115 KeV and H ions implantation with an energy of 75 KeV were carried out on 2-inch semi-insulating InP (100) wafers by sequence. Unless noted otherwise, He ions implantation was carried out before H ions implantation. He ions



Accepted Manuscript

1
2
3
4
5
6
7
8
9
10
11
12
13
14
15
16
17
18
19
20
21
22
23
24
25
26
27
28
29
30
31
32
33
34
35
36
37
38
39
40
41
42
43
44
45
46
47
48
49
50
51
52
53
54
55
56
57
58
59
60

implantation fluence was $2\times10^{16}$ cm$^{-2}$, while H ions implantation fluence varied from $3\times10^{16}$ cm$^{-2}$ to $7\times10^{16}$ cm$^{-2}$. Both He and H ions implantations were carried out at room temperature. In order to avoid the channeling effects, deliberate misalignment from the wafer normal of 7° was performed during the implantation processes. After implantations, the InP wafers were diced into small samples with the size of 10 mm×10 mm for the following characterizations. Some of the samples were annealed to achieve the surface blistering or exfoliation. The surface morphology of the samples was characterized by using an optical microscope (OM) of Leica DM4000M. The crystalline quality was examined by X-ray diffraction (XRD) with a Philips X'Pert X-ray diffractometer. The implantation-induced defects in the InP samples were determined by Rutherford backscattering spectroscopy (RBS) using 1.7 MeV He ions at a scatter angle of 170º and JEOL 2100F field-emission transmission electron microscopy (TEM). The cross-sectional scanning electron microscope (SEM) with Zeiss Supra55 was used to characterize the InP-on-Si structure.

**3. Results and Discussions**

After the He and H ions sequential implantation at room temperature, there is no significant change on the surface of the implanted InP (not shown). The surface blistering and exfoliation of the implanted InP occur after a post-annealing process at 150 °C for 1 hour. It is found that the implanted InP with varied H ions fluences show different exfoliation behaviors. The insets in Fig. 1 (a) show the OM images of the surface morphology for the He and H ions sequentially implanted InP with different H ions fluence. All the samples were post-annealed at 150 °C for 1 hour. At low H ions fluence of $3\times10^{16}$ cm$^{-2}$ no blistering or exfoliation was observed on the InP surface. Huge amounts of surface blistering appears as the H ions fluence was increased to $4\times10^{16}$ cm$^{-2}$, and the large area surface exfoliation starts when the fluence is increased to $5\times10^{16}$ cm$^{-2}$. Surprisingly, no blistering occurs on the sample surface implanted with the highest H ions fluence of $7\times10^{16}$ cm$^{-2}$. In order to quantificationally evaluate the InP exfoliation behavior, a parameter of exfoliation efficiency $A_{ex}$ was introduced to quantify the exfoliation [13]. The exfoliation efficiency is defined as $A_{ex}\% = \frac{A_{ex}^{total}}{A_{sample}^{total}} \cdot 100\%$, where $A_{ex}^{total}$ is the sum of the individual exfoliation areas, and $A_{sample}^{total}$ is the area of the entire OM image. Fig. 1 (a) shows the exfoliation efficiency of implanted InP with different H ions implantation fluence. With increasing H ions fluence, the exfoliation efficiency presents a Gaussian-like distribution and reaches a maximum value of 90.6% at H ions fluence of $5\times10^{16}$ cm$^{-2}$.

The exfoliation efficiency $A_{ex}$ is related to efficient exfoliation cavities introduced by the implanted ions [13]. With H ions fluence below $3\times10^{16}$ cm$^{-2}$, the internal pressure of the efficient exfoliation cavities induced by H ions implantation is limited. Thus, there is no surface

Accepted Manuscript

1
2
3
4
5
6
7
8
9
10
11
12
13
14
15
16
17
18
19
20
21
22
23
24
25
26
27
28
29
30
31
32
33
34
35
36
37
38
39
40
41
42
43
44
45
46
47
48
49
50
51
52
53
54
55
56
57
58
59
60

blistering or exfoliation observed on the InP surface even after the post-annealing process. By increasing the H ions fluence to $4\times10^{16}$ cm$^{-2}$, the internal pressure of the efficient exfoliation cavities is beyond the threshold for the surface blistering on the InP wafers. By further increasing the H ions fluence, a cleavage assisted coalescence between neighbor efficient exfoliation cavities occurs during the post-annealing process due to the large stress introduced by high fluence H ions implantation. And the internal pressure of the efficient exfoliation cavities is large enough to overcome the fracture stress of InP, which results in the large area surface exfoliation. In general, the nucleation of exfoliation efficiency cavities will be heightened with increasing H ions implantation fluence [14]. Hence, by increasing the H ions implantation fluence from $3\times10^{16}$ cm$^{-2}$ to $5\times10^{16}$ cm$^{-2}$, the exfoliation efficiency of InP increases. However, when the H ions implantation fluence is larger than $5\times10^{16}$ cm$^{-2}$, the exfoliation efficiency decreases with the increasing H ions implantation fluence. There is even no surface blistering or exfoliation observed on the InP crystal wafer with H ions fluence over $6\times10^{16}$ cm$^{-2}$. The similar exfoliation behaviors were also observed in Si by H and He ions sequential implantation [15].

In order to understand the underlying mechanism of the observed exfoliation behavior, the InP samples with He and H ions sequential implantation at room temperature (without the post-annealing process) were examined by XRD. Fig. 1 (b) shows the (ω/2θ) XRD scans along the InP (004) reflection. In comparison to the XRD curve of the virgin InP crystal wafer, the implanted InP samples present additional scattered intensity with fringe pattern for the angles lower than the Bragg's angle, which indicates that there is out-of-plane tensile strain gradient with Gassian-like shape induced by the ion implantation [16]. The periodicity of the fringe is related to the width of the strain layer and the most distant fringe from the Bragg's angle corresponds to the maximum stain in InP samples. Both the lattice parameters of the unstrained InP substrate and strained layer follow the Bragg's law: $\lambda=2\cdot d_{sub}\cdot\sin(\theta_{B,sub})$ for the unstrained InP substrate; and $\lambda=2\cdot d_{layer}\cdot\sin(\theta_{B,sub}+\Delta\theta)$ for the strained layer. $\lambda$ is the wavelength of the incident X-ray, $d_{sub}$ is the lattice parameter of the unstrained InP substrate, $d_{layer}$ is the strained lattice parameter of the strain layer, $\theta_{B,sub}$ is the Bragg's angle of the unstrained InP substrate, and the $\theta_{B,sub}+\Delta\theta$ is the Bragg's angle of the strained layer. Then, the strain $\varepsilon$ is expressed by equation (1) [16].

$$\varepsilon = \frac{d_{layer}-d_{sub}}{d_{sub}} = \frac{\sin(\theta_{B,sub})}{\sin(\theta_{B,sub}+\Delta\theta)} - 1 \quad (1)$$

Fig. 1 (c) shows the plot of maximum strain as a function of H ions fluence extracted from Fig. 1 (b). With the increase of the H ions fluence, the value of maximum strain first increases and then decreases as the H ions fluence is beyond $5\times10^{16}$ cm$^{-2}$, which is in the agreement with the results of the exfoliation efficiency shown by the red curve in Fig. 1 (a). It is well believed that the implantation induced lattice strain in the crystalline structure increases with increasing



Accepted Manuscript

1
2
3
4
5
6
7
8
9
10
11
12
13
14
15
16
17
18
19
20
21
22
23
24
25
26
27
28
29
30
31
32
33
34
35
36
37
38
39
40
41
42
43
44
45
46
47
48
49
50
51
52
53
54
55
56
57
58
59
60

implantation fluence. However, the implanted crystal will be partially decrystallized with excessive implantation [17], which releases the implantation lattice strain instead. Therefore, the maximum strain decreases when the H ions implantation fluence is over $5\times10^{16}$ cm$^{-2}$. It is reported that the implantation introduced out-of-plane strain promotes the nucleation and growth of platelet defects, meanwhile, out-of-plane strain is also a driving force for migration of platelet defects [18]. During the post-annealing process, the platelet defects migrate to coalesce with each other, which results in the surface exfoliation. As the H ions fluence beyond $5\times10^{16}$ cm$^{-2}$, the implantation induced strain is released and the growth and migration of the platelet defects are unmotivated, resulting in less exfoliations or even no exfoliation on the surface of samples after annealing.

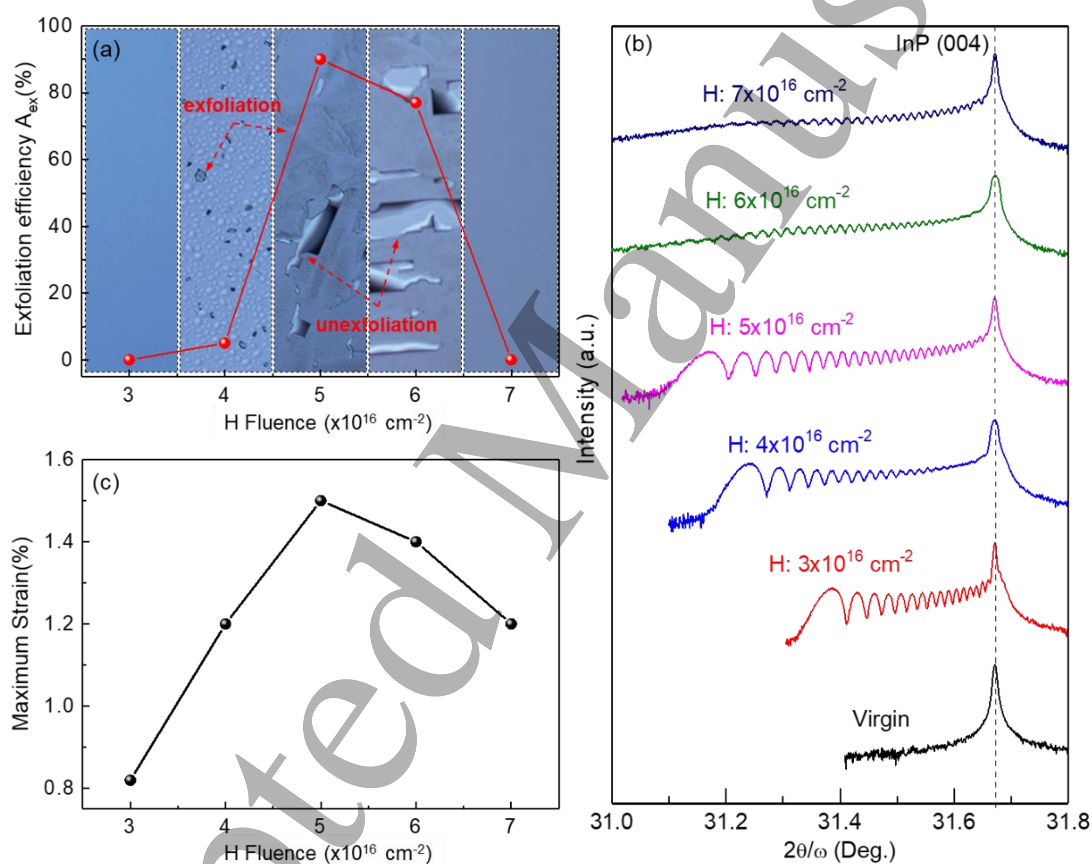


Fig. 1 (a) Exfoliation efficiency as a function of H ions implantation fluence for the He and H ions sequentially implanted InP after annealing at 150 °C for 1 hour. The insets show the corresponding OM images of the surface morphology. (b) ω-2θ scan XRD curves along the InP (004) reflection for He and H ions co-implanted InP with different H ions implantation fluence. (c) The maximum strain as a function of H ions implantation fluence extracted from the XRD measurements.

In addition to the implantation fluence, the implantation sequence of He and H ions has a



Accepted Manuscript

1
2
3
4
5
6
7
8
9
10
11
12
13
14
15
16
17
18
19
20
21
22
23
24
25
26
27
28
29
30
31
32
33
34
35
36
37
38
39
40
41
42
43
44
45
46
47
48
49
50
51
52
53
54
55
56
57
58
59
60

great influence on the InP surface blistering or exfoliation as well. Fig. 2 (a) and (b) show the OM images of the InP surface with different implantation sequence of He and H ions after a post-annealing at 150 °C for 1 hour. The He and H ions implantation fluences are $2\times10^{16}$ $cm^{-2}$ and $5\times10^{16}$ $cm^{-2}$, respectively. Large area exfoliation appears on the surface of sample pre-implanted with He ions as shown in Fig. 2 (a), but no exfoliation or blistering is observed on the surface of sample pre-implanted with H ions as shown in Fig. 2 (b). As shown in Fig. 2 (c), Rutherford backscattering spectroscopy (RBS) in channeling mode was performed to study the implantation-induced defects in the InP samples with different implantation sequence of He and H ions. For comparison, the random and channeling RBS spectra of the virgin InP sample are also presented. There is an evident damage peak at the channel number of 618 for all implanted InP samples. The damage peak for the samples pre-implanted with H ions is higher than that of the sample pre-implanted with He ions, which indicates that H ions pre-implantation followed by He ions implantation introduce heavier lattice damages in comparison with the case of He ions pre-implantation followed by H ions implantation. After post-annealing at 150°C for 6 min, the damage peak for the sample pre-implanted with He ions increases significantly, which suggests a defect evolution during the post-annealing process. However, there is no obvious change for the sample pre-implanted with H ions before and after the post-annealing process. As shown in Fig. 2 (d) and (e), cross-sectional TEM was utilized to analyze the microstructure around the mean projected range of the ion implantation for the implanted InP samples after post-annealing at 150 °C for 6 min. Some platelet defects, which are parallel to the surface of the samples, appear around the mean projected range of the ion implantation for InP sample pre-implanted with He ions as shown in Fig. 2 (d). He ions implantation with a relatively low fluence would create a certain amount of open volume defects as the H ions trapping layer in the InP crystal [19]. The subsequent implanted H ions can be attracted into the open volume defects and increase the internal pressure of the open volume defects. With post-annealing, the implanted H ions aggregate into the open volume defects due to the Oswald ripening effect, and facilitate the open volume defects growing up to be platelet defects. The nucleation and growth of platelet defects increase the dechanneling level, which results in the increase of the damage peak in RBS spectra for the sample pre-implanted with He ions [19-21]. Moreover, the platelet defects serve as the precursors of the micro-cracks which are essential for the surface exfoliation [22]. However, the platelets defect was not observed in the InP samples pre-implanted with H ions as shown in Fig. 2 (e). H ions implantation introduced mainly the tiny point defects, like vacancy or vacancy cluster, rather than the large open volume defects, e.g., bubble or cavity, in the InP crystal. The small point defects prevent the formation of the large open volume defects induced by the subsequent He ions implantation and obstruct the growth of continues platelet defects parallel to the InP crystal surface. Therefore, large area surface



Accepted Manuscript

1 2 3 4 5 6 7 8 9 10 11 12 13 14 15 16 17 18 19 20 21 22 23 24 25 26 27 28 29 30 31 32 33 34 35 36 37 38 39 40 41 42 43 44 45 46 47 48 49 50 51 52 53 54 55 56 57 58 59 60

exfoliation occurs in the sample pre-implanted with He ions as shown in Fig. 2 (a), but not in the sample pre-implanted with H ions as shown in Fig. 2 (b).

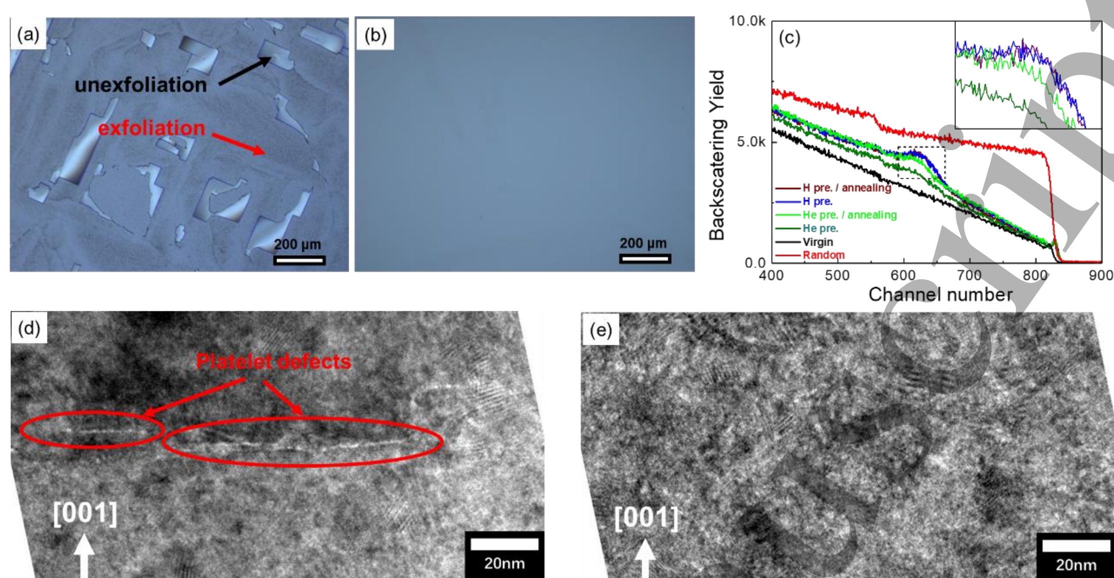


Fig. 2 OM images of the InP surface with different implantation sequence of He and H ions after a post-annealing at 150 °C for 1 hour. The He and H ions implantation fluences are $2\times10^{16}$ cm$^{-2}$ and $5\times10^{16}$ cm$^{-2}$, respectively. Large area exfoliation appears on the surface of sample pre-implanted with He ions (a), but no exfoliation or blistering was observed on the surface of sample pre-implanted with H ions (b). (c) RBS measurements for the InP samples with different implantation sequence of He and H ions. "Virgin" denotes the InP sample without ion implantation, "He pre." denotes the InP sample pre-implanted with He, "He pre. / annealing" denotes the InP sample pre-implanted with He ions and post-annealed at 150 °C for 1 hour, "H pre." denotes the InP sample pre-implanted with H, and "H pre. / annealing" denotes the InP sample pre-implanted with H ions and post-annealed at 150 °C for 6 min. Cross-sectional TEM images of the InP samples pre-implanted with He ions (d) and pre-implanted with H ions (e) after post-annealing 150 °C for 6 min.

A kinetics analysis of the thermally activated blistering process based on the Arrhenius relationship is essential to clarify the dependence of annealing parameters on the thermal evolution of blistering and exfoliations. The samples pre-implanted with He ions ($2\times10^{16}$ cm$^{-2}$) followed by H ions implantation ($5\times10^{16}$ cm$^{-2}$) were annealed with a Linkam THMS600 Temperature Controlled Stage and inspected in-suit with optical microscopy to determine the exfoliation time at different annealing temperature from 120 °C to 165 °C. Fig. 3 shows the Arrhenius plot of the exfoliation time as a function of reciprocal temperature in semi-log



Accepted Manuscript

1
2
3
4
5
6
7
8
9
10
11
12
13
14
15
16
17
18
19
20
21
22
23
24
25
26
27
28
29
30
31
32
33
34
35
36
37
38
39
40
41
42
43
44
45
46
47
48
49
50
51
52
53
54
55
56
57
58
59
60

coordinates, where longitudinal axis of the exfoliation time is in a log scale but the horizontal axis of reciprocal temperature is in a linear scale. Only one activation energy $E_a$=0.427 eV was extracted from the Arrhenius plot based on $1/t_b \propto \exp(-E_a/KT)$, where $t_b$ is the onset time to form exfoliation and K is Boltzmann's constant and T is the absolute temperature [23]. There is no transition temperature where the activation energy changes abruptly, which was observed the InP with only He ions implantation [10]. In the case of GaAs blistering induced by H and He ions sequential implantation, there is no transition temperature as well and only one activation energy was extracted [14]. In comparison with InP blistering induced by only He ions implantation at low temperature (−15 °C) [10], the InP blistering with He and H ions sequential implantation in this work requires much lower activation energy (0.740 eV in Ref. [10], but 0.427 eV in this work) and much lower exfoliation temperature (over 200 °C in Ref. [10], but below 165 °C in this work). This suggests that the He and H ions sequential implantation can reduce the InP thin film splitting thermal budget dramatically. Additionally, the low exfoliation temperature can reduce the thermal strain in the InP-on-Si hetero-integration materials.

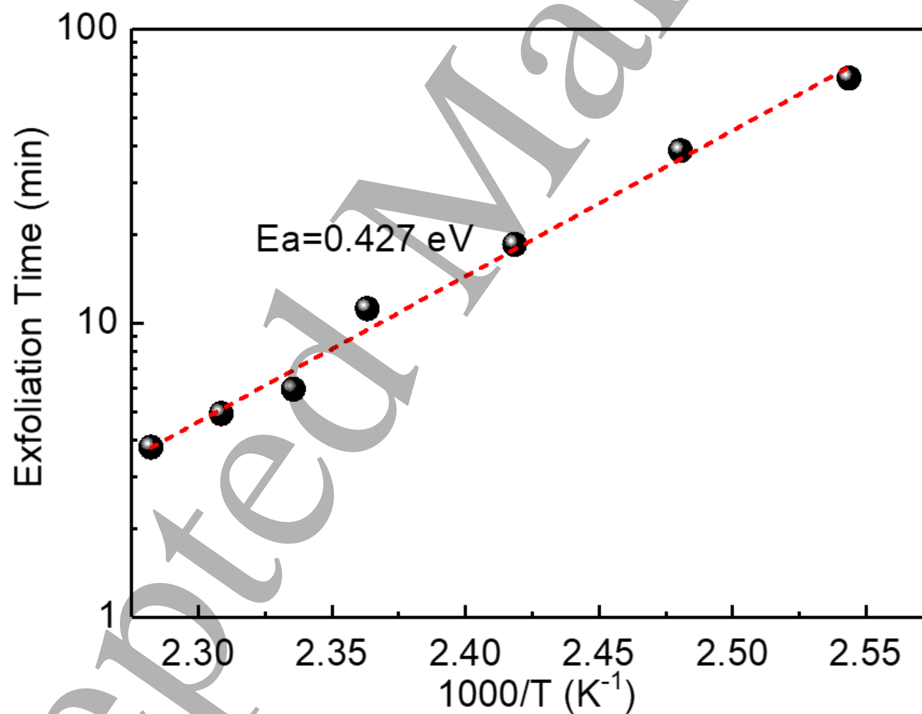


Fig. 3 Arrhenius plot of the exfoliation time as a function of reciprocal temperature for samples pre-implanted with He ions ($2\times10^{16}$ cm$^{-2}$) followed by H ions implantation ($5\times10^{16}$ cm$^{-2}$).

In order to achieve the wafer scale InP-on-Si hetero-integration, the He and H sequential implantation was carried out on a 2-inch InP wafer at room temperature. The ion energy/fluence of the He and H ions implantation are 115 KeV/$2\times10^{16}$ cm$^{-2}$ and 75 KeV/$5\times10^{16}$ cm$^{-2}$,



Accepted Manuscript

1
2
3
4
5
6
7
8
9
10
11
12
13
14
15
16
17
18
19
20
21
22
23
24
25
26
27
28
29
30
31
32
33
34
35
36
37
38
39
40
41
42
43
44
45
46
47
48
49
50
51
52
53
54
55
56
57
58
59
60

respectively. After the ion implantation and post-annealing, the surface blistering and exfoliation occurred at the free surface to release the stress longitudinally. However, when a stiffener is bonded onto the implanted crystal, the longitudinal relaxation of the stress is prevented, but the implantation induced micro-cracks grow laterally which could result in the fracture and delamination of the whole layer [24-26]. Therefore, the implanted InP wafer was bonded with a 4-inch $SiO_2$/Si(100) substrate directly. Subsequently, the bonding pair of InP/$SiO_2$/Si wafers was annealed at 150°C for 1 hour in $N_2$ atmosphere furnace. After annealing, a 2-inch InP layer was successfully transferred to the Si substrate as marked with dashed circle in Fig. 4 (a), and the 2-inch InP donor wafer was retained completely which can be recycled. A wafer-scale InP-on-Si hetero-integration material was prepared. Fig. 4 (b) shows a typical cross-sectional scanning electron microscope (SEM) image of the as-prepared InP-on-Si structure, which reveals a sharp and smooth interface between the InP layer and $SiO_2$/Si substrate. The total thickness of the transferred InP thin film is about 634 nm. The crystalline quality of the transferred InP thin film was evaluated by X-ray rocking curves (XRCs) measurements. The normalized (004) XRCs for the bulk InP substrate and as-transferred InP thin film are shown in Fig. 4 (c). The full width at half maximum (FWHM) of the XRC is 61 arcsec for the transferred InP, which is slightly higher than the value of the bulk InP substrate (16 arcsec). The broadened FWHM of transferred InP thin film is due to the implantation-induced lattice disorder and a damaged surface layer. This is commonly observed in the transferred thin film by ion-slicing process [27]. The profiles of the implantation induced damage (displacement per atom, DPA) simulated by SRIM 2008 [28] are shown in Fig. 4 (d). The red line indicates the DPA induced by the He and H ions sequential implantation performed in this work, while the black line is the DPA induced by single He implantation with a fluence of $5\times10^{16}$ $cm^{-2}$ [28]. Both DPA profiles show Gaussian-like distribution, and the peak of the profiles should be the exfoliation depth position. It is clear that the DPA induced by the He and H ions sequential implantation is only half of that for the single He ion implantation, which suggests that InP thin film with higher quality can be prepared by efficient ion-slicing process with the He and H ions sequential implantation. Moreover, the FWHM of the as-transferred InP thin film (61 arcsec) is even smaller than that of the heteroepitaxially grown InP thin film on patterned Si substrates (75-540 arcsec) [29,30]. The implantation-induced lattice disorder is possible to be recovered by an appropriate annealing process, and the damaged surface layer can be removed by a chemical mechanical polishing (CMP) process. Therefore, the quality of the transferred InP thin film can be further improved.



Accepted Manuscript

1 2 3 4 5 6 7 8 9 10 11 12 13 14 15 16 17 18 19 20 21 22 23 24 25 26 27 28 29 30 31 32 33 34 35 36 37 38 39 40 41 42 43 44 45 46 47 48 49 50 51 52 53 54 55 56 57 58 59 60

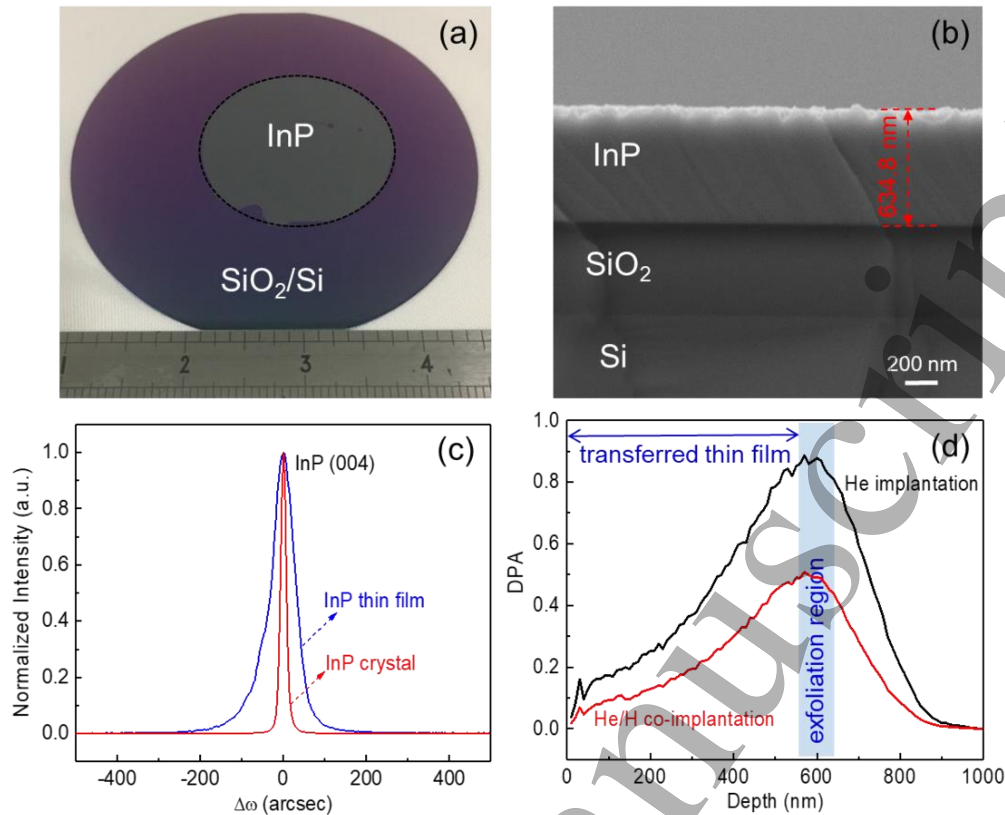


Fig. 4 (a) The image of 2-inch InP thin film transferred on $SiO_2$/Si substrate. The dashed circle roughs the area of the transferred InP thin film. (b) Typical cross-sectional SEM image of the as-prepared InP-on-Si hetero-integration material. (c) The normalized (004) XRCs for the virgin InP crystal and as-transferred InP thin film. (d) Implantation induced DPA profiles simulated by SRIM 2008.

**4. Conclusions**

In conclusion, we have demonstrated the efficient exfoliation of crystalline InP thin film by sequential implantation of He and H ions at room temperature. The thermal evolution of the implantation induced defects in InP crystals was investigated and the resulting surface blistering and exfoliation were characterized. With the increasing H ions implantation fluence, the exfoliation efficiency first increases and then decreases, which is consistent with implantation induced strain as revealed by XRD measurements. The surface exfoliation was only observed on the InP pre-implanted with He ions but not on the InP pre-implanted with H ions, which suggests that the sequence of He and H ions implantation plays a crucial role on the InP thin film splitting. The monolithic integration of high quality 2 inch InP thin film with 4 inch Si (100) substrate was achieved. The He and H ions sequential implantation can significantly reduce the InP thin film splitting thermal budget and introduce less implantation-induced defects in the transferred InP thin film. Efficient hetero-integration of InP on Si will serve as the platform for silicon-based photonic-electronic integration.



Accepted Manuscript

1
2
3
4
5
6
7
8
9
10
11
12
13
14
15
16
17
18
19
20
21
22
23
24
25
26
27
28
29
30
31
32
33
34
35
36
37
38
39
40
41
42
43
44
45
46
47
48
49
50
51
52
53
54
55
56
57
58
59
60

**Acknowledgements**

This work was supported by the National Natural Science Foundation of China (No.: 11705262, 11622545, U1732268 and 61674161), Frontier Science Key Program of CAS (No.: QYZDY-SSW-JSC032), One Hundred Talent Program of CAS, PuJiang Talent Program of Shanghai (No.: 17PJ1410500), International Collaboration Project of Shanghai (No.: 16520721100).

**References**

[1] Pasquariello D, Camacho M, Hjort K, Dózsa L and Szentpáli B 2001 Evaluation of InP-to-silicon heterobonding *Mater. Sci. Eng. B Solid-State Mater. Adv. Technol.* **80** 134–7

[2] Hjort K 2004 Transfer of InP epilayers by wafer bonding *J. Cryst. Growth* **268** 346–58

[3] Prucnal S, Zhou S, Ou X, Reuther H, Liedke M O, Mücklich A, Helm M, Zuk J, Turek M, Pyszniak K and Skorupa W 2012 InP nanocrystals on silicon for optoelectronic applications *Nanotechnology* **23** 485204

[4] Wuu D S, Horng R H and Lee M K 1990 Indium phosphide on silicon heteroepitaxy: Lattice deformation and strain relaxation *J. Appl. Phys.* **68** 3338–42

[5] Itakura H, Suzuki T, Jiang Z K, Soga T, Jimbo T and Umeno M 1991 Effect of InGaAs/InP strained layer superlattice in InP-on-Si *J. Cryst. Growth* **115** 154–7

[6] Moutanabbir O and Gösele U 2010 Heterogeneous Integration of Compound Semiconductors *Annu. Rev. Mater. Res.* **40** 469–500

[7] Bruel M 1995 Silicon on insulator material technology Electron. Lett.**31** 1201

[8] Dharmarasu N, Sundarakkannan B, Kesavamoorthy R, Nair K G M and Kumar J 1999 Investigations on $H^+$ and $He^+$ implantation effects in n-InP using Raman scattering *Phys. B Condens. Matter* **262** 329–35

[9] Hayashi S, Bruno D and Goorsky M S 2004 Temperature dependence of hydrogen-induced exfoliation of InP *Appl. Phys. Lett.* **85** 236–8

[10] Singh R, Radu I, Scholz R, Himcinschi C, Gösele U and Christiansen S H 2006 Investigation of helium implantation induced blistering in InP *J. Lumin.* **121** 379–82

[11] Chen P, Di Z, Nastasi M, Bruno E, Grimaldi M G, Theodore N D and Lau S S 2008 Effects of hydrogen implantation temperature on InP surface blistering *Appl. Phys.*



Accepted Manuscript

*Lett.* **92** 14–7

[12] Singh R, Radu I, Scholz R, Himcinschi C, Gösele U and Christiansen S H 2006 Low temperature InP layer transfer onto Si by helium implantation and direct wafer bonding *Semicond. Sci. Technol.* **21** 1311–4

[13] Zhang L and Li B S 2017 Study of surface exfoliation on 6H-SiC induced by $H_2^+$ implantation *Phys. B Condens. Matter* **508** 104–11

[14] Woo H J, Choi H W, Kim G D, Kim J K and Kim K J 2009 Blistering/exfoliation kinetics of GaAs by hydrogen and helium implantations *Surf. Coatings Technol.* **203** 2370–4

[15] Reboh S, Schaurich F, Declemy A, Barbot J F, Beaufort M F, Cherkashin N and Fichtner P F P 2010 On the microstructure of Si coimplanted with $H^+$ and $He^+$ ions at moderate energies *J. Appl. Phys.* **108**

[16] Moulet C and Goorsky M S 2012 Lattice Strain Measurements in Hydrogen Implanted Materials for Layer Transfer Processes *Ion Implant.* 65–88

[17] Jia Q, Huang K, You T, Yi A, Lin J, Zhang S, Zhou M, Zhang B, Zhang B, Yu W, Ou X and Wang X 2018 Freestanding ultrathin single-crystalline SiC substrate by MeV H ion-slicing *Appl. Phys. Lett.* **112**

[18] Nastasi M, Höchbauer T, Lee J K, Misra A, Hirth J P, Ridgway M and Lafford T 2005 Nucleation and growth of platelets in hydrogen-ion-implanted silicon *Appl. Phys. Lett.* **86** 1–3

[19] Weldon M K, Collot M, Chabal Y J, Venezia V C, Agarwal A, Haynes T E, Eaglesham D J, Christman S B and Chaban E E 1998 Mechanism of silicon exfoliation induced by hydrogen/helium co-implantation *Appl. Phys. Lett.* **73** 3721–3

[20] Grisolia J, Cristiano F, De Mauduit B, Assayag G Ben, Letertre F, Aspar B, Di Cioccio L and Claverie A 2000 Kinetic aspects of the growth of hydrogen induced platelets in SiC *J. Appl. Phys.* **87** 8415–9

[21] Li B S, Zhang C H, Zhang H H, Shibayama T and Yang Y T 2011 Study of the damage produced in 6H-SiC by He irradiation *Vacuum* **86** 452–6

[22] Li B S, Wang Z G and Jin J F 2013 Implantation temperature and thermal annealing

Accepted Manuscript

1
2
3
4
5
6
7
8
9
10
11
12
13
14
15
16
17
18
19
20
21
22
23
24
25
26
27
28
29
30
31
32
33
34
35
36
37
38
39
40
41
42
43
44
45
46
47
48
49
50
51
52
53
54
55
56
57
58
59
60

behavior in H2+-implanted 6H-SiC *Nucl. Instruments Methods Phys. Res. Sect. B Beam Interact. with Mater. Atoms* **316** 239–44

[23] Tong Q Y, Gutjahr K, Hopfe S, Gösele U and Lee T H 1997 Layer splitting process in hydrogen-implanted Si, Ge, SiC, and diamond substrates *Appl. Phys. Lett.* **70** 1390–2

[24] Radu I, Szafraniak I, Scholz R, Alexe M and Gösele U 2003 Low-temperature layer splitting of (100) GaAs by He+H coimplantation and direct wafer bonding *Appl. Phys. Lett.* **82** 2413–5

[25] Fontcuberta I Morral A, Zahler J M, Griggs M J, Atwater H A and Chabal Y J 2005 Spectroscopic studies of the mechanism for hydrogen-induced exfoliation of InP *Phys. Rev. B - Condens. Matter Mater. Phys.* **72** 1–8

[26] Daghbouj N, Cherkashin N and Claverie A 2018 A method to determine the pressure and densities of gas stored in blisters: Application to H and He sequential ion implantation in silicon *Microelectron. Eng.* **190** 54–6

[27] Huang K, Jia Q, You T, Zhang R, Lin J, Zhang S, Zhou M, Zhang B, Yu W, Ou X and Wang X 2017 Investigation on thermodynamics of ion-slicing of GaN and heterogeneously integrating high-quality GaN films on CMOS compatible Si(100) substrates *Sci. Rep.* **7** 1–9

[28] Egeland G W, Valdez J A, Maloy S A, McClellan K J, Sickafus K E and Bond G M 2013 Heavy-ion irradiation defect accumulation in ZrN characterized by TEM, GIXRD, nanoindentation, and helium desorption *J. Nucl. Mater.* **435** 77–87

[29] Bakin A, Piester D, Behrens I, Wehmann H H, Peiner E, Ivanov A, Fehly D and Schlachetzki A 2003 Growth of InP layers on nanometer-scale patterned Si substrates *Cryst. Growth Des.* **3** 89–93

[30] Merckling C, Waldron N, Jiang S, Guo W, Collaert N, Caymax M, Vancoille E, Barla K, Thean A, Heyns M and Vandervorst W 2014 Heteroepitaxy of InP on Si(001) by selective-area metal organic vapor-phase epitaxy in sub-50 nm width trenches: The role of the nucleation layer and the recess engineering *J. Appl. Phys.* **115** 1–7



Accepted Manuscript